INCREASE THE PACKING DENSITY OF VERTICALLY ALIGNED CARBON NANOTUBE ARRAY FOR THE APPLICATION OF THERMAL INTERFACE MATERIALS

A Thesis
Presented to
The Academic Faculty

By

Wentian Gu

In Partial Fufillment
Of the Requirement for the Degree
Master of Materials Science and Engineering

August, 2011

INCREASE THE PACKING DENSITY OF VERTICALLY ALIGNED CARBON NANOTUBE ARRAY FOR THE APPLICATION OF THERMAL INTERFACE MATERIALS

Approved by:

Dr. C. P. Wong, Advisor
School of Materials Science and Engineering
Georgia Institute of Technology

Dr. Robert L. Snyder
School of Materials Science and Engineering
Georgia Institute of Technology

Dr. Meilin Liu
School of Materials Science and Engineering
Georgia Institute of Technology

Date approved: March 7, 2011

I dedicate this work to my family and friends, especially my Mom and my girlfriend for their support

ACKNOWLEDGEMENTS

I would like to start by thanking everyone who has helped me through my research and study. A special thanks to my advisor Dr. C. P. Wong for his guidance and support. He gave me the opportunity to study and learn at a fine institute. Working with him was a great experience in an environment that was both challenging and fun. Thank you to my committee members, Dr. Robert L. Snyder and Dr. Meilin Liu, for taking the time to help me in the final step in this chapter of my life.

I would like to thank for the financial support from DARPA during the completion of my research. Thanks to Wei Lin, Yagang Yao and other seniors in the group for their helpful guidance along with allowing me to get familiar with the research work and to complete my studies.

To my family, thank you Mom and Dad for your support and tolerating all of my stressful moments at Tech. Thank you Di for not only being my girlfriend, but also a cheerleader in my life who is always full of courage.

Finally, thank you to all of my friends who have always been there for me, I will never forget you guys.

TABLE OF CONTENTS

LIST OF TABLES

LIST OF FIGURES

LIST OF SYMBOLS AND ABBREVIATIONS

SEM	Scanning electronic microscope
TEM	Tunneling electronic microscope
TGA	Thermal gravimetric analysis
LFA	Laser Flash analysis
CNT	Carbon nanotube
VACNT	Vertically aligned carbon nanotube
CVD	Chemical vapor deposition
κ	Thermal conductivity
α	Thermal diffusivity
ρ	Mass density
c_p	Specific heat capacity

SUMMARY

The work of this thesis is focused on increasing the packing density of vertically aligned carbon nanotube (VACNT) array for its application in thermal interface materials (TIMs). Chemical vapor deposition method is applied for the synthesis of the VACNT array. The packing density is increased by applying cycled deposition of catalyst layers. As a prerequisite for the discussion about the role of packing density played in the thermal conductivity of VACNT array, the method to keep the quality and the thickness of the samples uniform is also discussed.

Through the use of scanning electronic microscope (SEM) and tunneling electronic microscope (TEM) the morphology of the CNT samples were determined. The quality data of the samples are characterized by thermal gravimetric analysis (TGA) and Raman spectra. The thermal diffusivity values of the samples are obtained by modified Laser Flash analysis (LFA), and the thermal conductivity values are easily calculated based on the thermal diffusivity results.

The result shows that the VACNT arrays with higher packing density tend to be more thermal conductive. Liquid precursor can be applied to increase the growth rate of CNTs, but excess amount of liquid precursor may lead to degradation of the quality of the samples. With the thickness of 500 microns, the optimized thermal conductivity of VACNT array reaches 75.5 W/m K, which is about 3 times the value of a sample grown under ordinary conditions. This work is believed to be a step closer to the fulfillment of the potential of VACNT array as TIMs.

Chapter 1 INTRODUCTION

1.1 Introduction

This thesis will evaluate the effect of the packing density of vertically aligned carbon nanotube (VACNT) array on its thermal conductivity, which is a step closer to the application of VACNT in the thermal interface materials (TIMs). To fully understand the results obtained during the study of the VACNT synthesis, some background information is offered. The thesis will begin by discussing VACNT array, what it is and its potential is to be used as TIMs. Subsequently, an overview of the synthesis methods for VACNT array and their mechanisms will be presented.

To interpret and understand the results, this thesis will give an overview of Laser Flash Analysis (LFA), which is used to measure the thermal conductivity of the samples in the experiment with some minor modifications. The basic ideas of the characterizations for the quality and the packing density of VACNT array will be introduced in **Chapter 3** and **Chapter 4**.

1.1.1 Carbon nanotube (CNT)

Carbon nanotube is one of the most exciting nanomaterials. In 1991, Iijima (NEC Laboratory) first reported the observation of multi-walled CNTs (MWNTs) [2]. Since then, intensive studies about the structure, properties, and potential applications of CNTs

have been performed. In 1993, single-walled CNTs (SWNTs) were observed. The theoretical studies predicted the extraordinary mechanical, electronic and thermal properties of the CNTs, which makes this material promising in a wide range of applications. Among these predictions, the most striking one is that CNTs could be either metallic or semiconducting, depending on their diameter and chiral angle. This prediction was later verified experimentally by STM in 1998 [3, 4], opening a possibility of CNT based electronics.

The structure of single-walled CNT can be illustrated clearly in its 2D pattern. Geometrically, CNT can be formed by "bending" a single layer graphene into the cylindrical shape and then "sewing" the seam perfectly. The direction of "bending" determines the chirality of the CNT. In the 2D pattern, this direction can be defined by the vectors C_h and T, as shown in **Figure 1.1**. These two vectors can always be expressed in the form of combination of two unit vectors a_1 and a_2 in the 2D pattern: $C_h = na_1 + ma_2$, where n and m are integers. The chiral angle θ is determined relative to the direction defined by a_1. Different types of CNTs have different values of n and m, making them varied in chirality and diameter, and therefore, electrical properties. Specifically, SWNTs are metallic if |n-m|=3q and those for which |n-m|=3q±1 are semiconducting, where q is an integer. Zigzag nanotubes correspond to (n, 0) or (0, m) and have a chiral angle of 0°, armchair nanotubes have (n, n) and a chiral angle of 30°, while chiral CNTs have general (n, m) values and a chiral angle of between 0° and 30°. The geometry of the graphene lattice and the chiral vector of the tube determine the structural parameters, such as diameter, unit cell, and number of carbon atoms. The diameter of the nanotube is given by

$$d = \frac{|C_h|}{\pi} = \frac{\sqrt{3}a_{C-C}\sqrt{n^2+nm+m^2}}{\pi} \quad (equation\ 1.1)$$

where $a_{C\text{-}C}$ is the C-C bond length (1.42 Å).

The structure of MWNT is consisted of concentric SWNTs, with the average distance of 0.34 nm between neighboring walls, which is similar to the distance between neighboring layers of graphite.

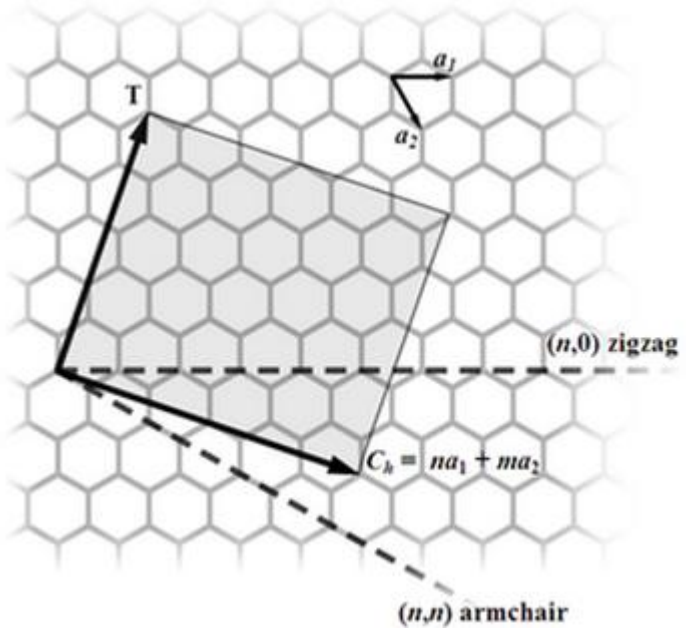

Figure 1.1 The illustration of C_h vector in the 2D graphene structure

1.1.2 Vertically aligned CNT (VACNT) array

VACNT array is advantageous over randomly oriented CNTs for its isotropic properties, controlled and patterned growth. Typically, VACNT array is formed by simultaneous rapid growth of many CNTs in confined space. The alignment of the CNTs is a steric effect. During the growth process, the CNTs are aligned by Van de Waals force

between neighboring CNTs. VACNT array is evaluated by its thickness, quality (concentration of defects), packing density and its interaction/adhesion with the substrate (easiness of transfer). Researchers have reported several methods for the synthesis of VACNT array, which will be present in **section 1.2**.

1.2 Synthesis of CNTs

In general, CNTs can be grown by arc-discharge, laser ablation and chemical vapor deposition (CVD) methods, among which CVD method is the most popular one for large yield, aligned and selective spatial growth.

1.2.1 Arc-discharge method

Arc discharge method is distinguished from other methods by providing both single wall and multi wall CNTs of the highest crystallinity. In this method, plasma of inert gas is excited by high electric current passing the space between opposing carbon electrodes. Carbon atoms are then evaporated by the plasma, and deposit into other carbon structures. This method was originally proposed for the synthesis of fullerene. In 1992, Ebbesen and Ajayan adapted this method to synthesize MWNTs in a large scale under a helium atmosphere [1]. Based on their results, the purity and yield of MWNTs obtained using this method are strongly dependent on the gas pressure in the reaction vessel. The length of the synthesized MWNTs is about several microns with diameters ranging from 2 to 20 nm. The product maintains high crystallinity (**Figure 1.1**). However, carbon particles were always observed on the sidewall of synthesized MWNTs, undermining the merit of arc-discharge as a meaningful synthesis method for high purity CNTs. In 1993, arc-discharge synthesis of SWNT was reported. However, the product

was still always accompanied with abundant fullerene particles. To get high purity CNTs, further purification of the product is unavoidable.

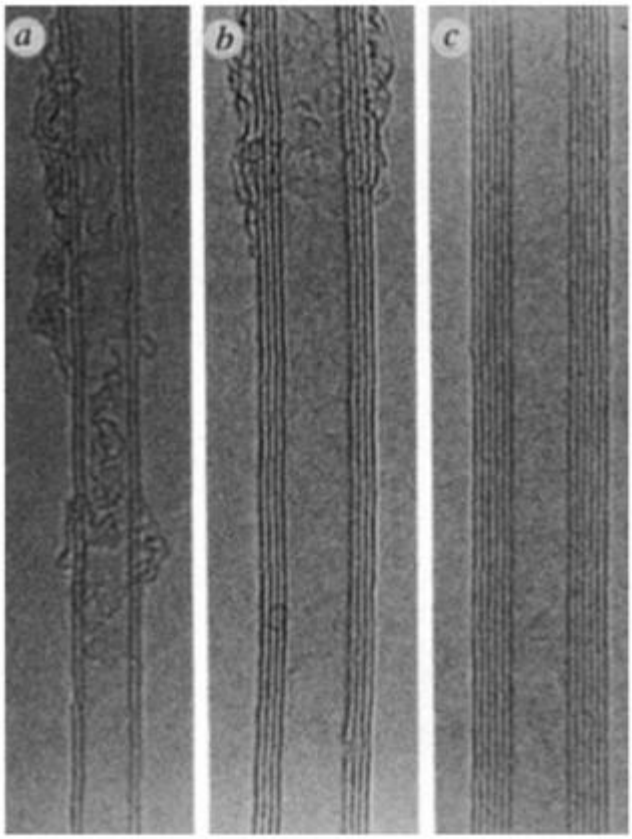

Figure 1.2 TEM images of CNTs with different diameters synthesized by arc-discharge method [1].

1.2.2 Laser ablation method

This method was first reported by Smalley group in 1996. In this method, double pulse lasers are applied to evaporate graphite rods doped with 1.2% atomic 1:1 Co/Ni powders. The graphite rod was heated up to 1200 ℃ in the furnace under Ar flow. The pressure was kept at 500 Torr. This process was followed by heat treatment in vacuum at

1000 ℃ to remove fullerenes and other carbon structures as byproducts (**Figure 1.1**). The SWNTs produced were aggregated in bundles by Van de Waals force.

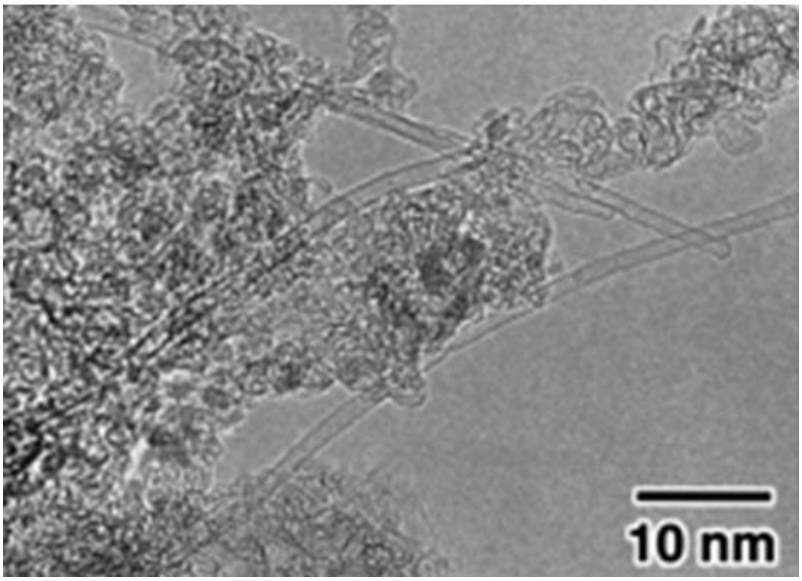

Figure 1.3 TEM image of CNTs synthesized by laser ablation method [4]

The availability of high quality CNTs from arc-discharge and laser ablation method provides the essential prerequisite for fundamental studies of the structures and properties of CNTs. However, these two methods meet up with some critical difficulties in the real life application. For example, the temperature needed for the synthesis is too high, usually around 3000 ℃, which greatly increases the cost. Besides, the CNTs synthesized by these methods are often aggregated and entangled, which makes the purification, manipulation and assembly extremely difficult. Furthermore, as mentioned above, various kinds of carbon species such as amorphous carbon and fullerenes are produced as byproducts and attached on the sidewalls of CNTs, which is unavoidable.

1.2.3 Chemical vapor deposition (CVD)

A detailed discussion about the catalyzed growth of CNTs by chemical vapor deposition (CVD) is necessary, because it offers a promising route to bulk production of high-purity CNTs that can be scaled-up to VACNT array. The conventional CVD process is called thermal CVD method, because the energy needed to decompose the precursor is provided by heat. In a typical CNT growth process, transition metal (Fe, Co, Ni etc.) films are deposited on the surface of the substrate as the catalyst. As the substrate is heated up, the thin film cracks into small islands. Given fixed amount of metal deposited on the growth substrate, the number and average size of catalyst particles is strongly dependent on the conditions of the heat pretreatment. Then the hydrocarbon precursor is conducted in the furnace to start the CNT growth. After the CNT growth, the precursor flow is terminated and the sample is cooled down naturally to room temperature in the reducing atmosphere (Ar/H_2). The typical set up of conventional CVD method is illustrated in **Figure 1.1**.

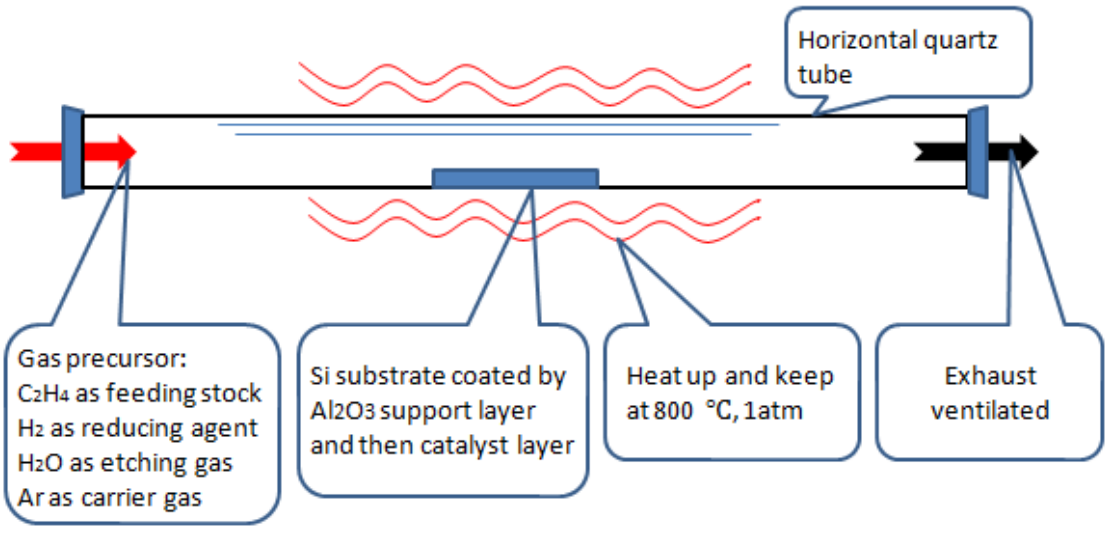

Figure 1.4 Typical set up of conventional CVD system

Thermal CVD process is very sensitive to various factors, including growth temperature, pressure, gas flow rates, the design of reaction chamber, introduction of hetero-elements (H, S, O, etc.) and so on [5].

First of all, growth temperature is always an important factor in all kinds of chemical reactions. There is a distribution of temperature in the reaction chamber. The temperature profile depends on the heating method and the design of reaction chamber. G Y Xiong [6] and coworkers reported that the temperature at which metal oxide layer is reduced to pure metal catalyst determines the size of resulting catalyst particles. In addition, the growth temperature is reported to be strongly related to the diameter and chirality of CNTs [7].This result is quite important in our research, because the spacing between neighboring CNTs, which can be directly derived from the diameter of CNTs given a constant packing density, strongly affects the diffusivity of the carbon source.

Being aware of the role temperature plays in CNT growth, the importance of controlling the pressure in the CVD system can be quite intuitive. The pressure affects the heat dissipation from the reaction sites during CNT growth. A higher pressure would slow down the heat dissipation and maintain a higher local temperature at reaction sites compared to the atmosphere and vice versa. The local temperature of reaction sites needs to be in a critical range for a higher rate of carbon condensation.

Besides the temperature and pressure in the reaction system, the recipe of gas precursor is also critical. In the CNT growth, the gas precursor consists mainly of carbon source (CH_4, C_2H_4, C_2H_2, etc.), hydrogen, carrier gas (He, N_2, Ar, etc.) and, in some cases, water vapor and/or NH_3. The gases have different effects on the CNT growth.

Various hydrocarbon species have been applied as carbon source for CNT growth, including ethylene, acetylene, xylene, ethanol, etc. Inorganic carbon source, such as CO and CO_2, are also applied. It has been acknowledged that acetylene is the direct building block for CNT structure [8]. At a fixed temperature, the rate of pyrolysis varies for different carbon sources. Both too high and too low decomposition rate are not desirable for the formation of CNT. If the carbon source decomposes too fast, amorphous carbon would rapidly form and spread on the surface of catalyst. On the contrary, a too low decomposition rate would cause a lack of carbon in the initial stage. Besides the concern about the rate of pyrolysis, it is also reported that carbon sources containing oxygen (CO [9], C_2H_5OH [10] etc.) perform uniquely in CNT growth, because oxygen atoms can oxidize the redundant amorphous carbon and extend the lifetime of catalyst. Since different carbon sources vary in self diffusivity, we apply ethylene as carbon source in all series of experiments.

The role of hydrogen in CNT growth process is complicated. At around 500 ℃, hydrogen starts to reduce metal oxide to pure metal catalyst. During the steady growth stage, however, hydrogen etches away redundant amorphous carbon in the form of radicals. Researchers have revealed that H_2O can assist the synthesis of ultra-long CNTs [11], which turned out to be due to the synergic effects of H and O atoms in etching.

Inert gases (N_2, Ar, He) are applied in CNT growth process as carrier gas. Carrier gas can adjust the concentration and the flow rate of the effective recipe. Since absolute sealing is hard to achieve, carrier gas can also provide protective atmosphere for the reduction of catalyst and the formation of CNTs. Besides, similar to the effect of pressure

on the CNT growth, the carrier gases have influence on the heat dissipation of reaction sites, because different carrier gases vary in heat capacity and thermal conductivity.

Thermal CVD method is the most popular process for high yield and quality CNT production. Besides thermal CVD, there are several other CVD processes for CNT synthesis.

PECVD method was originally proposed as an alternative to thermal CVD for lower temperature growth of silicon, its oxide and nitride, and other materials in integrated circuit manufacturing. The low temperature processing is because of the energy contribution from high energy electrons for chemical reactions in the gas or plasma phase. This method was later introduced into the growth of CNT, with a hope of decreasing the reaction temperature. Indeed PECVD method brings down the growth temperature by 100-200℃ compared to thermal-CVD method. Typically, the reactor for PECVD method consists of two parallel plate electrodes, equal in area, housed inside a vacuum chamber. The upper electrode is grounded and the lower electrode is connected to a dc power supply. A mechanical pump is applied to provide operating pressures of a few torrs. A gas showerhead at the top electrode provides uniform flow over the substrate. The lower electrode consists of a resistive heater assembly to independently heat the substrate, regardless of the plasma heating effects. High density reactive plasmas are induced by radio-frequency (rf) source.

Although the growth temperature is brought down, the resulting material quality is not as good as those from high temperature processes. This tradeoff is not unique for CNT, but is similar to that seen in the case of many other materials grown by PECVD as well. Large amounts of impurities scatter in the product. The byproduct of amorphous

carbon greatly enhances the adhesion of the VACNT array to the substrate, which makes the transfer much more difficult.

Liquid precursor CVD has also been proposed as a major CVD method for CNT growth. This method best fits in the mass production of CNTs, because of higher growth rate and easy process. In this method, conventional gas precursor is replaced with liquid precursor, such as hexane, xylene, benzene, etc. The catalyst of the reaction is also provided in the liquid. Organometallic compounds, such as ferrocene, are dissolved into the liquid precursor as catalyst. At the growth temperature, the liquid solution is injected into the reaction tube at a constant rate by syringe. Both the liquid precursor and the organometallic compound quickly decompose at the growth temperature and metal-carbon core shell structured particles are created. These particles join with each other by combining the carbon shells into nanotubes. As a result, the CNTs grown from liquid precursor often have discrete metal particles trapped inside the hollow (**Figure 1.1**). The detailed discussion about liquid precursor CVD process will be presented in **section 4.1**.

Liquid precursor CVD also has its shortcomings. Firstly, the catalyst is not predefined at certain local sites, but contained in the liquid. As a result, the synthesized CNTs cannot be grown on selected sites, in other words, patterned growth of CNTs is unavailable. The purity of the VACNT array synthesized using this method is also lower, because redundant amorphous carbon would reside in the space between neighboring CNTs. Some carbon species even bond on the sidewall of CNTs and disrupt the regular sp^2 hexagonal arrangement of carbon atoms, bringing sp^3 bonds. Besides, the reagents related to liquid precursor CVD are toxic, which greatly undermines its value in real life applications.

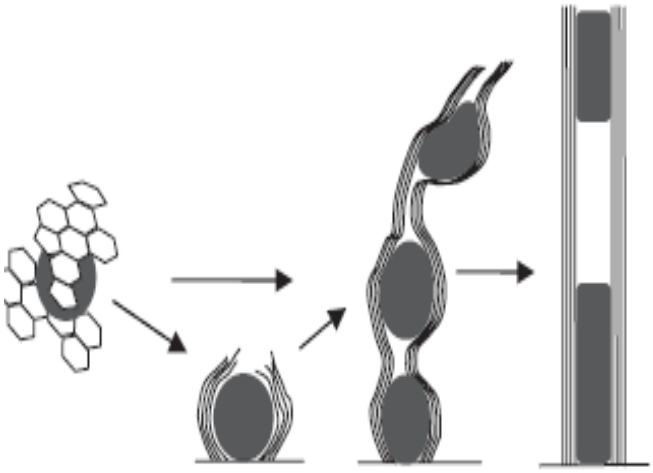

Figure 1.5 The illustration of the mechanism of VACNT growth supported by liquid precursor

1.3. Mechanism of VACNT array growth

As is widely acknowledged, mechanism for CNT growth has been generally assumed to be a dissociation-diffusion-precipitation process during which elemental carbon is formed on the surface of a metal catalyst particle followed by diffusion and precipitation in the form of cylindrical graphite [12].

As a classical way to explain the process of CNT growth, vapor-liquid-solid (VLS) model was first proposed [13] by Y. Saito and further developed and named [14] by J. Gavillet. According to VLS model, dissociated carbon reaches and dissolves into the "liquid" catalyst particle. Liquid catalyst particles form at the growth temperature due to the melting point depression effect originated from the small particle size. As the temperature drops, the solubility of carbon in the catalyst particle decreases dramatically, and carbon begins to precipitate on the particle surface and nucleates for the growth of CNTs; CNT growth is due to a continuous diffusion of carbon from the exposed catalyst

surface through the particle. The path of CNT formation according to VLS model is illustrated in **Figure 1.1**. It was thought that the diffusion of carbon through the catalyst particle is the rate-limiting step in the steady growth.

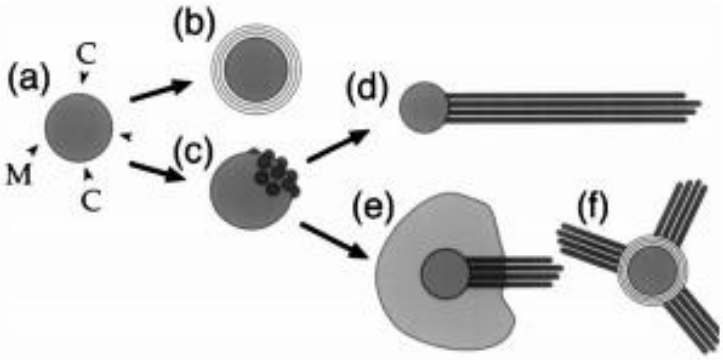

Figure 1.6 The proposed path of CNT formation in VLS model [14]

Although VLS model is still widely appreciated by now, there are still several issues open to debate: (1) the path of dissociated carbon from the atmosphere to the surface of catalyst is not clear. This issue is closely related to the mass transfer problem; (2) the nature of the driving force for the carbon diffusion in the catalyst particle is not discussed; (3) the mechanism of CNT growth termination needs more detailed description.

To address the first problem, Lingbo Zhu [15] monitored the growth of CNT array by formation of CNT stacks. CNT stacks were made by intermittent carbon source supply and showed the CNT growth at different periods of time. He found that when the temperature was above 740 ℃, the lengths of CNTs decreased with time; while when the temperature was below 740 ℃ the lengths of CNTs in all stacks were roughly the same (**Figure 1.1**). Zhu therefore proposed that the length of CNT should be diffusion controlled above 740 ℃ while reaction rate controlled below 740 ℃. It was considered

that the concentration of carbon source on the top of CNTs was higher than that on the root. Therefore, the dissociated carbon was concentration driven to diffuse from the top to the root, where the catalyst particles were present. Zhu proposed that in the diffusion controlled process, as the CNT stacks accumulated, the diffusion flow of carbon decreased exponentially; while in the reaction rate controlled process, the reaction rate stayed roughly the same throughout the process, which results in CNT stacks with uniform thickness. Jie Liu indirectly supported this theory as he proposed "Kite mechanism" [16], in which floating catalyst particles on the tip of CNTs were considered more effective than those attached on the support layer.

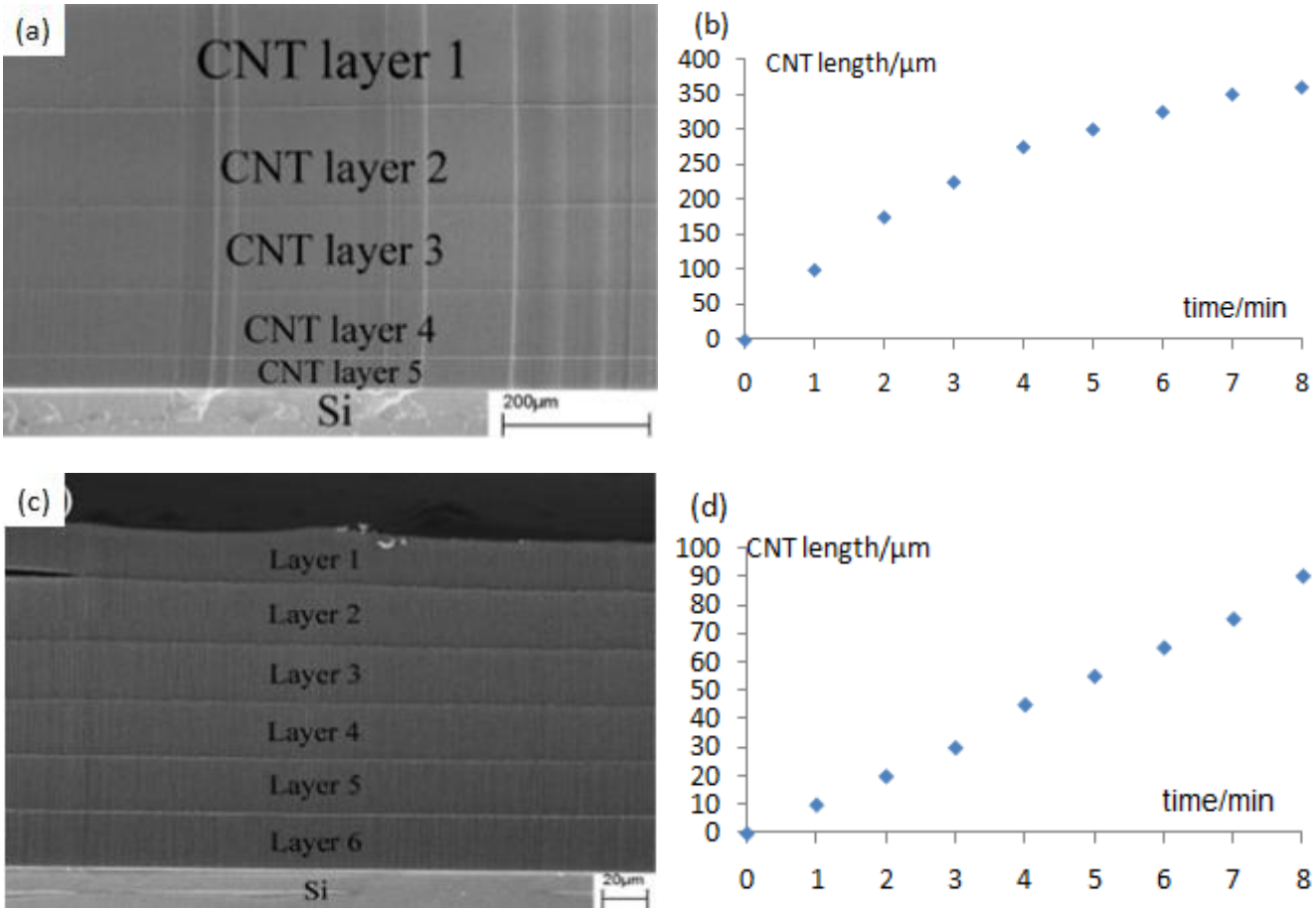

Figure 1.7 The CNT stack layers grown (a) over 740℃; (b) under 740℃[15]

Now we focus on the discussion about the type of diffusion and the driving force. Baker et al. proposed that a temperature gradient across the catalyst particle was the driving force for the carbon diffusion [17]. It was believed that carbon diffused from the hotter leading surface on which the exothermic pyrolysis of hydrocarbons occurs to the cooler surfaces on which carbon is precipitated endothermically. There is some experimental evidence for the temperature-driven carbon diffusion mechanism[18, 19], nevertheless, the model could not provide a rational explanation for the endothermic pyrolysis of some hydrocarbons such as methane.

Alternatively, concentration-driven diffusion mechanism was proposed by Nielsen *et al* [20]. This model involves a concentration gradient across the catalyst particle in contact with the hydrocarbon on one side and with a graphitic precipitation on the other side. However, they failed to provide any experimental evidence as support for this model.

Both temperature-driven and concentration-driven diffusion mechanisms assume bulk diffusion of carbon through catalyst. Against any bulk diffusion model, a surface diffusion model was first proposed by Baird in 1974 [21], which was found to be more satisfactory and consistent for both platelet and filamentary graphitic carbon deposit on catalyst surface. At the beginning stage, a clean "liquid-like" catalyst particle formed on the surface of the supporting material as a result of reduction of catalyst oxide by hydrogen at elevated temperatures. An association of metal and hydrocarbon species then nucleated on the fresh surface of the liquid catalyst particle and diffuses on the surface and dissociates at the contact angle between the droplet and the wall of the supporting material. The subsequent further precipitation of carbon gives rise to the graphitic shell.

In comparison with bulk diffusion of carbon into the catalyst particle, which seems unlikely due to high activation energy, a surface diffusion process seems more feasible. Furthermore, Puretzki *et al.* consider that carbon forms a highly disordered "molten" layer on the surface of catalyst. This disordered structure can provide greater carbon diffusivity on the surface.

It is inconclusive which diffusion mechanism is the most effective, but these mechanisms tend to work competitively and synergistically. Recently, N. Latorre *et al.*[22] proposed a combination of bulk diffusion and surface diffusion. They considered that carbon diffused from "a clean surface" (interface 1 in **Figure 1.1**) through both bulk and surface to the active sites (interface 2) and got added into CNT structure.

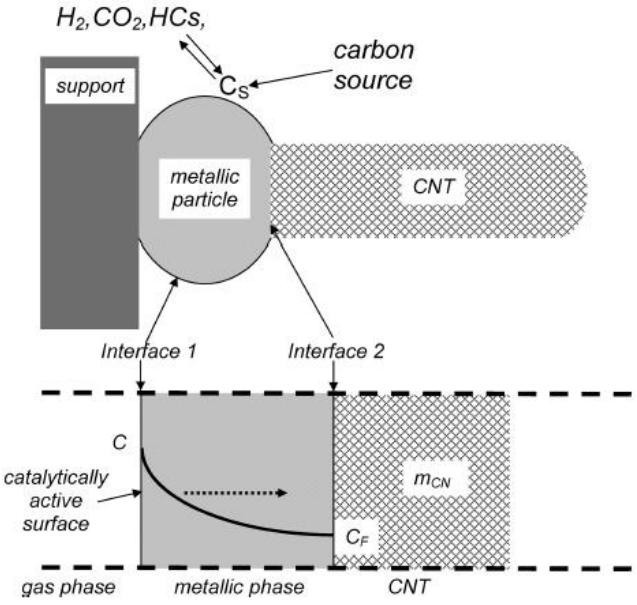

Figure 1.8 Carbon diffusion process proposed by N. Latorre [22]

As for the last problem, the opinions get more diverse. At first, many efforts were made to avoid the termination in CNT array growth. Researchers adjusted the recipe of gas

mixture to mediate gas phase reactions and prolong the duration of catalyst activity [23-26]. CNT array growth is also prolonged by adjusting the stoichiometry of bimetallic catalyst particles [26] and by stabilizing the underlying Al_2O_3 support by doping with a rare earth element such as La [27]. Yet termination of CNT array growth has not been overcome.

Researchers believe that the reason for the termination of CNT growth varies with different systems. One typical reason is the deactivation of catalyst. The deactivation is often caused by carbon encapsulation on the surface of catalyst particles, or "poisoning" of catalyst. A. I. La Cava [28] first described the process of metal catalyzed carbon deposition. In this process, hydrocarbon was either irreversibly adsorbed on the metal surface or converted to aromatic species in the gas phase. The aromatic species formed in the atmosphere tended to be attached on the metal particles and encapsulate them. The hydrocarbon which originally adsorbed on the particles dehydrated and formed catalytic fibrous whisker or contributed to the encapsulation of the particles. Iijima [29] proposed that growth termination was due to formation of polyhedral capping or conical capping on the open end of CNTs. He believed that the open end lays active sites for addition of carbon atoms into CNT structure. The caps develop fast whenever conditions are not appropriate for steady growth, and they consume all the active sites for carbon addition to the CNT structure. However, if tip growth mode applies in this case, the "capping" proposed by Iijima would also serve to encapsulate catalyst particles and therefore terminate CNT growth.

Another reason for CNT array growth termination was proposed to be the cessation of detectable carbon diffusion from atmosphere to catalyst surface. Maruyama

and co-workers [30] analyzed the feedstock diffusion limitations in the CNT growth process and found that the diffusion would limit the growth kinetics when the arrays grew to the lengths of 400 μm. This opinion lies on an assumption that the mass transfer is along the top-down direction.

There are also some other models for CNT array growth termination. Jae-Hee Han *et al* [31] established a model in which CNT growth termination was caused by interaction between neighboring CNTs. With a small fluctuation in length, the growth of further longer CNT was suppressed by the Vander Waal's force between itself and neighboring shorter CNTs. Recently, Mostafa[32] proposed that the termination was due to a sudden loss of alignment at the root of CNT array. All these models found some experimental evidence to support themselves.

1.4. Thermal conductivity of individual CNT and VACNT array

1.4.1. Thermal conductivity of individual CNT

High thermal conductivity (κ) is one of the most attractive intrinsic properties of carbon nanotubes [33]. In 2000, Berber *et al.* [34] first calculated κ of an individual SWNT to be ~6600 W m^{-1} K^{-1} based on molecular dynamic simulation. Such a high κ is mainly attributed to the large mean free path of phonons in CNT. Based on theoretical discussions, κ of individual CNTs should be related to tube diameter [34, 35], length[36], chirality [37], defect [38], and temperature [39], *etc*.

Experimental κ values of individual CNTs were later reported, falling in a wide range of 42-3000 W m^{-1} K^{-1} [40, 41]. The scattering data is caused by the non-uniformity of the measurement and nanotube parameters.

1.4.2. Collective thermal conductivity of VACNT array

For practical applications, collective thermal transport property of 1-D CNT aggregates are of more interest than the intrinsic κ of individual CNTs and collective thermal transport property of 2-D and 3-D random CNT networks [42]. Hone *et al*. reported κ of ~250 W m^{-1} K^{-1} for a magnetically aligned single-walled CNT film [43]. Yang *et al*. found that κ of a vertically aligned CNT (VACNT) array by a microwave plasma enhanced chemical vapor deposition (PECVD) process was only 12-17 W m^{-1} K^{-1} [44]. They attributed the low κ to the small packing density of CNTs in the array. Yi *et al*. measured κ of millimeter-long aligned multi-walled CNTs. At room temperature, κ was only ~25 W m^{-1} K^{-1}. The relatively low value was attributed hypothetically to a substantial amount of CNT defects. Wang *et al.* used a photothermal technique to measure the thermal conductivity of carbon nanofiber arrays and revealed a relatively low κ of ~27 W m^{-1} K^{-1} [45]. κ of 74-83 W m^{-1} K^{-1} for a VACNT array (13 um, multi-walled CNTs with a bamboo-like structure by microwave PECVD) in the temperature range of 295-323 K was reported by Hu *et al*. using a 3ω measurement technique [46].

With recent success on large-scale synthesis of VACNTs by various CVD processes, VACNTs have found a promising application as thermal interface materials (TIMs) for electronic packaging. Hu *et al.* used a 3ω method to test the thermal contact resistance between a 13-μm thick VACNT array and the surface of a free mating substrate. The results showed that the contact resistances were 17 and 15 mm^2 K W^{-1}, respectively, under the pressure of 0.040 and 0.100 MPa [46]. Ngo *et al.* used electrodeposited Cu as a gap filler to enhance the stability and thermal transport of carbon nanofibers [47]. They reported the interfacial thermal resistance of 25 mm^2 K W^{-1} under a

pressure of 0.414 MPa with a one-dimensional reference bar method. Using a similar characterization method, Xu and Fisher reported an interfacial thermal resistance of 19.8 mm^2 K W^{-1} for a VACNT array at 0.45 MPa. By using a phase change material (PCM) with the VACNTs, they obtained a minimum resistance of 5.2 mm^2 K W^{-1}. Xu *et al*. used a photothermal method to evaluate the effective thermal resistance of VACNT arrays grown on Si substrates by PECVD [48]. The resistance was 12-16 mm^2 K W^{-1}, comparable to the resistance of commercially available thermal grease. Zhu *et al.* used a photothermal technique to measure the contact resistance of a VACNT/solder interface and estimate the thermal conductivity of the VACNT array. The κ was 81 W m^{-1} K^{-1}. However, the VACNT/solder contact resistance was large (43 mm^2 K W^{-1}). Tong *et al.* grew a 7-μm thick VACNT array on Si and dry-attached the VACNT/Si to a glass plate. They used a transient phase sensitive photothermal technique to measure the VACNT/glass interfacial resistance to be 11 mm^2 K W^{-1} [49]. Cola *et al.* reported an overall resistance of 16 mm^2 K W^{-1} at 0.241 MPa for a Si/15-μm-VACNT/silver TIM measured by a photoacoustic technique. They fabricated an interface material comprised of a metal foil with CNTs synthesized on both sides of the foil. This fabrication lowered the overall interfacial resistance to less than 10 mm^2 K W^{-1} [50]. Furthermore, they grew VACNTs on Si and Cu substrates and fabricated them to make a two-sided VACNT TIM layer. By this assembly, they reported a minimum resistance of 4 mm^2 K W^{-1}. Hu *et al.* used an IR microscopy technique to measure the thermal resistance of a VACNT-based interface with opposing VACNT arrays [51], which is essentially the same structure with the two-sided VACNT TIM layer in ref. 49. However, they found a very large thermal resistance across the array-to-array contact interface, ~140 mm^2 K W^{-1}, which is in a

sharp contrast with the result in ref. 49. Panzer *et al*. used a thermoreflectance technique to measure the thermal resistance of a 28-μm-thick surface-metalized VACNT array synthesized on a Si substrate. The overall resistance was 12 mm^2 K W^{-1}, dominated by the contact resistance due to the small fraction of CNTs in the array that is in contact with the mating substrate [52]. Recently, Lin *et al*. developed a chemical anchoring process to assemble VACNT TIMs [53]. An overall thermal resistance of ~10 mm^2 K W^{-1} was estimated by a laser flash technique.

1.5. Thermal interface materials

One of the most attractive applications of VACNT array is thermal interface materials (TIMs) in microelectronic devices. With the exponential enhancement of the level of integration in microelectronic systems, heat dissipation becomes a critical problem for smaller and smarter devices. Heat spreaders are designed and applied to transfer heat generated from the functional parts (chips) to the outside packaging area. Since air is poor in thermal conductivity, TIMs are needed to fill in the gap between the chip and the heat spreader, so that the heat can be transferred (**Figure 1.1**). Besides the thermal conductivity, there are several other essential factors to be concerned in TIMs design. TIMs should be flexible enough to conform with the surface morphology of the chip and the heat spreader, so that a good contact can be ensured. Besides, TIMs should be mechanically strong to resist possible cracks. Furthermore, TIMs should be small in the thermal expansion coefficient, so that when they are heated up, negligible deformation is caused.

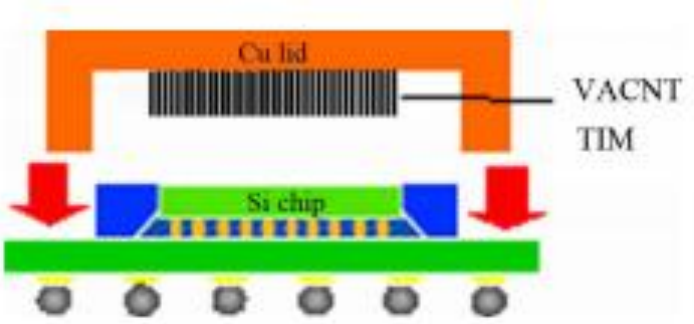

Figure 1.9 The location of VACNT TIMs in packaging [54]

Concerning all these factors, CNT is quite a promising candidate for the TIMs applications. It is mechanically strong and highly conductive, which is better than polymer composite based TIMs, and the same with conventional solder TIMs. CNT is more flexible than solder TIMs. VACNT array can better conform to different surfaces than conventional solder TIMs. The thermal expansion coefficient of solder is so high that heating can cause a significant deformation. What's worse, because of the high modulus of solder metal, the deformation may cause the damage of the underlying chips, which is a severe reliability issue. Meanwhile, the thermal expansion coefficient of VACNT array is relatively small, and the individual CNTs are allowed to bend freely within the confined space, which guarantees the survival of the chips. In summary, it is of great significance to study CNTs as TIMs.

1.6. Packing density of VACNT array

The packing density of VACNT array is defined as the number of individual CNTs in a unit area. It is also often represented by the filling factor, which means fraction of CNT occupation in a unit area (in percentage). The packing density of VACNT array is strongly dependent on the areal density of the catalyst particles on the growth substrate

right before the CNT growth. In a typical CNT growth process, transition metal (Fe, Co, Ni etc.) films are deposited on the surface of the substrate as the catalyst. As the substrate is heated up, the thin film cracks into small islands. Given fixed amount of metal deposited on the growth substrate, the number and average size of catalyst particles is strongly dependent on the conditions of the heat pretreatment. The areal density of the catalyst particles right before CNT growth is the upper limit of the areal density of resulting CNTs, because some catalyst particles are not active as catalyst. Therefore, how to increase the areal density of VACNT array is studied, as summarized below.

1.6.1. The effect of Hydrogen

The effect of hydrogen in the heat treatment has been systematically studied. Nessim et al. found that the duration of hydrogen flow in the heat treatment poses impact on the packing density of resulting CNTs [54]. John Hart et al. extended this conclusion and claimed that the concentration of H_2 in the gas flow decides the initial activity of the catalyst particles [55], which is related to the growth rate of CNTs. The quality of the CNTs produced is guaranteed. However, the increase in the packing density is quite trivial.

1.6.2. Suppression of Ostwald Ripening

When the catalyst particles are formed, they are slightly different in size. The bigger ones are thermal dynamically more stable than smaller ones, because of smaller curvature on the surface. As the result, the bigger particles tend to grow while the smaller ones are likely to migrate toward and finally join into bigger ones. This phenomenon is named as Ostwald ripening. Ostwald ripening not only decreases the number of available

catalyst particles, but also makes the metal particles too big to be active as catalyst [56]. To address this problem, several methods are proposed to suppress the migration of catalyst nanoparticles. For example, introducing trace amount of water vapor during the heat treatment process is proposed [24]. In this way, the surface of the growth substrate is expected to be functionalized with hydroxyl groups. These functional groups lower the surface energy and prevent the metal nanoparticles from moving freely on the surface. It is also reported to suppress Ostwald ripening by strengthening the bonding between catalyst nanoparticles and the underneath barrier layer (typically Al_2O_3) by posting intense oxidation of the catalyst particles. In this way, Fe nanoparticles are oxidized into Fe_2O_3 while maintaining their geometric shape. Fe_2O_3 is more strongly bonded on Al_2O_3 than Fe. As a result, the average size of the catalyst particles is reduced to 1-3 nm, sometimes producing single wall nanotube (SWNT) arrays.

1.6.3. Molybdenum as conditioning catalyst

The addition of Mo as conditioning catalyst was first applied in the synthesis of single walled carbon nanotubes (SWNTs) [57]. The role of Mo is manifold. Some researchers reported the effect of Mo in stabilizing Fe catalyst nanoparticles at the annealing process. The formation of more stable $FeMoO_4$ phase is also reported [58]. At a high temperature, $FeMoO_4$ slowly decomposes into Fe, MoO_3 and Mo in the reducing atmosphere. Fe is slowly released from the complex phase so that catalyst agglomeration is avoided. MoO_3 is also reported to assist the decomposition of hydrocarbon during CNT growth process [59]. The introduction of Mo as assist-catalyst can reduce the size and increase the number of catalyst nanoparticles simultaneously. The shortcoming is that the

introduction of Mo may cause contamination of the furnace, posing negative impact on the reliability of the experimental result and the quality of the product.

1.7. Laser flash analysis (LFA)

The study of thermal transport relies on a consistent measurement of thermal conductivity. Laser flash analysis (LFA) is a sensitive non-contact transient thermal measurement technique, which is first proposed by Parker *et al.* in 1961[60]. In a typical LFA setup, a laser flash lamp, a sample and an infrared detector are vertically arranged. The flash lamp sends out a laser pulse on the front face of the sample. Meanwhile, the temperature on the rear surface of the sample is monitored by the infrared detector. The time-resolved temperature evolution on the rear surface of the sample is recorded to fit into pre-set models to get the diffusivity (α) of the sample. The thermal conductivity (κ) of the sample is therefore calculated based on the definition: $\kappa=\alpha\rho c_p$, where ρ and c_p are mass density and specific heat, respectively. The allowable range of α is 0.01-1000 mm^2 s^{-1} for LFA 447, with a reproducibility of approximately ±3%. κ of the sample can be calculated based on the definition: $\kappa=\alpha\rho c_p$, where ρ and c_p are mass density and specific heat, respectively. LFA technique has recently been considered a tool to measure α of VACNTs and VACNT-based TIMs [53]. However, the feasibility is still controversial in view of the porous structure of VACNTs and usually large interfacial thermal resistance between CNTs and substrates. In our experiments, modified LFA is performed for the measurement of collective thermal conductivity of VACNT array, which will be explained in detail in **section 3.4**.

Chapter 2 MOTIVATION

Although VACNT array is considered one of the most promising candidates for the next generation TIMs, there is yet long way to go for fulfilling its potential. One of the most essential issues is the tradeoff between higher packing density and lower concentration of defects. By now, the filling factor of VACNT array in a unit area is still confined to below 5% for thermal CVD method. As a result, even if the individual CNT is qualified enough to show a high κ of over 500 W m^{-1} K^{-1}, the collective thermal conductivity of the VACNT array is only around 20-30 W m^{-1} K^{-1}. As mentioned in previous sections, other CVD methods were proposed for higher packing density of VACNT array, aiming to a higher collective thermal conductivity. The filling factor reaches as high as 40%-60% using PECVD method. However, no measurement of κ is conducted in any of these works. This is probably because that the plasma applied in PECVD method inducts many defects into the CNT structure and greatly degrades the quality of individual CNTs. On the other hand, some reported works even theoretically predict a decrease in κ with the packing density. The decrease is caused by the coupling effect between CNTs. The coupling effect modifies the phonon mode at the cross-section part of two contacting individual CNTs and makes the local sites thermally insulating [42]. In summary, the impact of packing density on the thermal conductivity of VACNT array given the same quality is still open to debate.

On the other hand, based on the brief review presented in **section 1.4.2**, the measurement methods for collective κ of VACNT array applied in different experimental

works are far from uniform, which lie difficulties in comparing and evaluating the results. Thus a consistent and reliable measurement is the prerequisite for any studies concerning the thermal transport of CNTs.

In the sense of this, the goal of this work is to (1) synthesize closely packed VACNT array without degrading the quality, using cycled deposition of catalyst; (2) quantitatively study the impact of packing density of VACNT array on its collective thermal conductivity, with consistent measurement. Thermal CVD method will be modified and optimized for higher packing density. The packing density is characterized by different methods to ensure the accuracy. The thermal conductivity of VACNT array is measured by modified laser flash method, which will be introduced in detail in **Chapter 3**.

For consistent and high yield production of CNTs, the growth rate of VACNT array is also studied. The effect of replacing gas precursor with liquid precursor is discussed. The total amount of catalyst used in cycled deposition process is also varied for optimized growth rate of VACNT array.

The systematic study of the relationship between the packing density of VACNT array and its thermal conductivity will provide a roadmap for CNT based TIMs design, that is, the optimized balance between the packing density and the quality of synthesized VACNT array. The evolution of growth rate with the amount of catalyst will also reveal the mechanism of CNT growth, which helps for high efficiency CNT growth. This work is a step closer to the real life application of VACNT array in TIMs.

Chapter 3 EXPERIMENTAL SECTION

3.1. Cycled deposition of the catalyst

Cycled deposition of the catalyst is proposed for increasing the areal density of catalyst nanoparticles for CNT growth. The process is illustrated in **Figure 1.1**. Si wafer is first oxidized in Lindberg Furnace to have a 200 nm thick oxidation layer on the surface. Then 10 nm Al is deposited on the oxidized wafer in the electron beam evaporator. The oxidation layer and the Al layer serve as barrier layers to prevent the poisoning of Fe catalyst caused by the interaction with underlying bulk Si. A thin film of Fe with predefined thickness is then deposited on the surface of the substrate. The catalyst thin film is annealed at 750 ℃ for 5 min to get cracked into small particles with a narrow size distribution. To prevent these nanoparticles from agglomerating in the following steps, a deep oxidation is performed at 300 ℃ in air so that a shell of Fe_2O_3 is formed on the surface of the particles. The interaction between the nanoparticles and the underlying Al_2O_3 layer is therefore strengthened. Then repeated deposition, annealing and deep oxidation are performed to make multilayer catalyst. The newly formed nanoparticles from latter cycles are expected to fill in the gap between the nanoparticles from the former cycles. In the first set of experiments, while the total thickness of the multilayer catalyst is fixed at 2 nm, the number of cycles and the thickness per cycle are varied. In the second set, the total thickness is varied to study the influence of the amount of catalyst on the growth rate. Here the thickness of the catalyst is calibrated by both

atomic force microscope (AFM) and the profilometer. The results are presented in **section 4.2**.

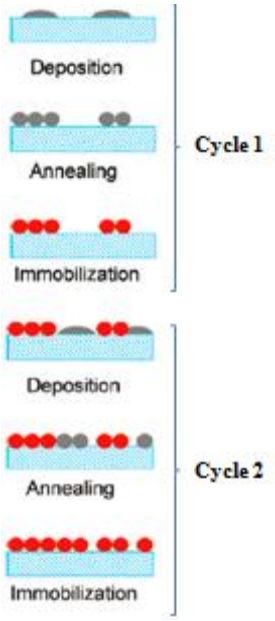

Figure 3.1 Cycled catalyst deposition

3.2. CVD synthesis of VACNT array

VACNT array is synthesized by thermal CVD method. The experiment set up of this method is shown in **Figure 1.4**. Typically, an Al_2O_3 tube is located in the tubular furnace. The catalyst coated substrate is pushed to the center of the tube. The reaction tube is then heated up to 750℃ at the rate of 25℃/min. The catalyst is annealed at 750℃under Ar/H_2 flow (670sccm/180sccm). As soon as the last cycle of annealing is finished, the hydrocarbon precursor (C_2H_4, 150sccm) is conducted into the reaction tube and CNT growth begins. The time for CNT growth is fixed as 15 min. After the CNT growth, the product is naturally cooled down under Ar/H_2 flow till below 300℃, so that the product may get rid of being attacked by the oxygen in the air. In the liquid precursor CVD process, there are two modifications compared with thermal CVD process. Firstly, the growth time is fixed at 5 min. Secondly, additional liquid precursor, xylene solution of ferrocene (wt% = 6.82%), is injected into the reaction tube at 750℃. The time for liquid precursor injection is varied from 0-5 min, to study the effect of liquid precursor on the growth rate.

3.3. Characterization

3.3.1. The packing density

The characterization of the packing density of VACNT array is challenging, because the tips of individual CNTs are not directly exposed to the vertical top view, sometimes even intertwined or entangled. Here several methods to convincingly characterize the packing density of VACNT array are applied, as presented below.

(1) Measurement of weight gain

Based on the average wall number (n) and inner diameter (d_i) of individual CNTs (**Figure 1.1**) from TEM image, the theoretical areal density of CNTs can be calculated (s = distance between neighboring CNT walls, typically s = 0.34nm):

$$\rho_{theory} = \rho_{graphite} \frac{\pi[(\frac{d_i}{2} + ns)^2 - (\frac{d_i}{2})^2]}{2\sqrt{3}(\frac{d_i}{2} + ns)^2} \quad (equation\ 3.1)$$

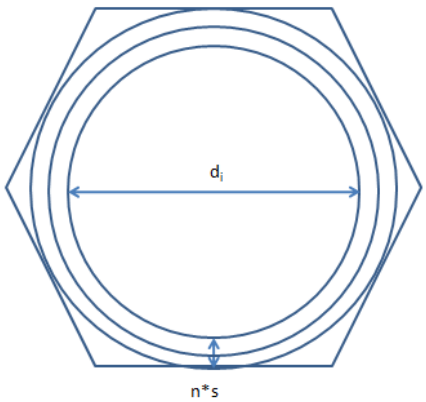

Figure 3.2 Individual CNT in a unit area (closely packing condition)

The thickness (l) and the net mass (m) of CNT array can be measured by SEM and microbalance respectively. Therefore, the filling percentage (p%) is:

$$p\% = \frac{m}{Al\rho_{theory}} \quad (equation\ 3.2)$$

where A is the total area of growth substrate.

(2) Observation of catalyst particles

As mentioned in the previous sections, the areal density of catalyst particles is the upper limit of the areal density of resulting CNTs. As-annealed catalyst particles are observed by scanning electronic microscope (SEM) to show the size and density profile.

(3) Indirect methods

VACNTs are found to shrink drastically with a drop of water on the tip. This is because the infiltration of water into the space between neighboring CNTs can cause strong capillary force which contract the CNT array to the theoretical packing density. Therefore, the original packing density of CNT array can be told by comparing the visional area the CNT array occupies before and after the water induced compaction. This method cannot provide quantitative results, however, because the extent of compaction is related to the original packing density.

Besides, the packing density of CNT array has impact on the hydrophobicity of the top surface. Contact angle characterization will be performed to indirectly evaluate the packing density. Although quantitative relation between the packing density and the

contact angle is still unavailable, the result can serve as an intuitive sign of density increase.

3.3.2. The quality

The quality of the VACNT array is evaluated by thermal gravimetric analysis (TGA) and Raman spectra.

In the process of TGA, the VACNT array is detached from the growth substrate and then gathered in a small vehicle. The CNTs are heated up at the rate of 10 ℃ min^{-1} under 10 sccm air flow, during which the weight of the sample is in-situ monitored by microbalance. The temperature at which sharp weight loss happens is taken as a criterion to evaluate the quality of the sample. The higher the temperature is, the better the quality of the sample.

Raman spectra characterize the type of bonding in sample species by detecting the vibration of the molecules. The Raman spectra of CNTs often contain two characteristic peaks: D peak and G peak. G peak is related to sp^2 hybridized bonding between carbon atoms, which is the normal arrangement of carbon atoms in the CNT structure. D peak is related to sp^3 hybridized bonding, which is abnormal in the structure of CNT, indicating the existence of defects or impurities. Therefore, the D/G peak intensity ratio is also taken as evidence of the quality of the sample. In our experiment, 532 nm laser is applied for Raman spectra. The incident laser shines on the top of the VACNT array. The spectra are taken from different spots for accuracy. The final result is the average of several observations.

3.4. Modified LFA for collective κ of the VACNT array

The LFA calculation is based on the following essential approximations:

(1) The heat flow in the sample is one-dimensional;

(2) The laser incidence and energy absorption can be considered instantaneous. In other words, pulse width of the incident laser is much shorter than the transit duration of the heat flow through the sample;

(3) Penetration depth of the incident laser is very small;

(4) Temperature change is small during the measurement process, so that α and c_p of the sample is kept constant;

(5) Heat losses from the sample surfaces are negligible.

In the case of VACNT array, it is geometrically porous and inhomogeneous. If the free-standing VACNT array is directly used as LFA sample, the incident laser will penetrate through the vacant spaces in the array or scattered away from the rough surface. Thus to meet both approximations (1) and (3), a thin gold coating is necessary to ensure rapid planar heat distribution upon the laser incidence. To minimize the reflectance of the laser, the gold coating is further coated with carbon to enhance the absorbance of the thermal energy. To satisfy approximation (4), α is obtained by extrapolating to zero incident laser pulse energy on the plot of apparent α values as a function of incident laser pulse energy. The results provided by modified LFA match well with already proved IR measurement.

Chapter 4 RESULTS AND DISCUSSIONS

4.1. The effect of liquid precursor

With the growth time fixed at 5 min, liquid precursor is injected into the reaction tube in the first 1-5 min. The growth rate of VACNT array is greatly enhanced by applying additional liquid precursor during the growth process. By adding liquid precursor in the first 1 min, the thickness of VACNT array is doubled compared to the one grown without extra catalyst (**Figure 1.1**). For the convenience of discussion, we name the samples as shown in table 4.1.

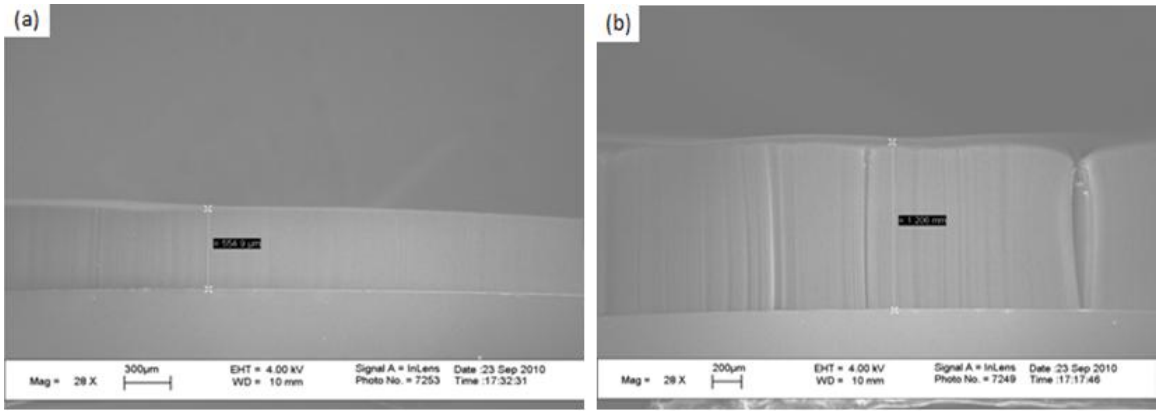

Figure 4.1 Low magnitude SEM images of (a) p-CNT; (b) 1min-CNT

Table 4.1 Nomenclature of the samples for the effect of liquid precursor

Sample name	description
p-CNT	The sample grown without extra liquid precursor
xylene-CNT	The sample grown with only xylene in the first 1 min
1min-CNT	The sample grown with liquid precursor in the first 1 min
2min-CNT	The sample grown with liquid precursor in the first 2 min
5min-CNT	The sample grown with liquid precursor throughout the 5min

A closer observation (**Figure 1.1**) reveals that, while the tips of individual CNTs are clean in p-CNT, all the samples grown with extra catalyst bare particles or clusters on the tip of the sample. Energy dispersive X-ray spectra (EDS) analysis shows that these particles are consisted of pure carbon. Note that the samples grown with extra catalyst are free from any particles on the sidewall of CNT array. Furthermore, by intentionally opening a slot on the side surface of the CNT array, it can be assured that no such particles or aggregates exist in between the neighboring individual CNTs. This feature does not match with typical liquid precursor CVD method [61]. As is widely known, in the typical liquid precursor CVD system, where no gas precursor is applied, the liquid precursor decomposes at high temperature and produces Fe nanoparticles wrapped by polycyclic aromatic hydrocarbons (PAHs). When the liquid precursor excesses the necessary amount, the produced PAH shelled Fe particles are no longer integrated into the CNT structure, but are often found filled in the space between neighboring individual CNTs or attached on the sidewalls of CNTs. In our system, as the amount of liquid precursor increases, more particles on the tips are observed, and they tend to agglomerate. This fact indicates two possibilities: (1) The decomposition of the liquid precursor

provides extra nucleis on the growth substrate. These nucleis develop into individual CNTs; (2) The Fe particles from the decomposition of the liquid precursor are all integrated into the CNT structure until the CNT growth expires, and then the following Fe particles deposit on the tips of the CNTs. However, the areal packing density of MWNT array is not obviously promoted by applying liquid precursor, thus the first possibility is eliminated.

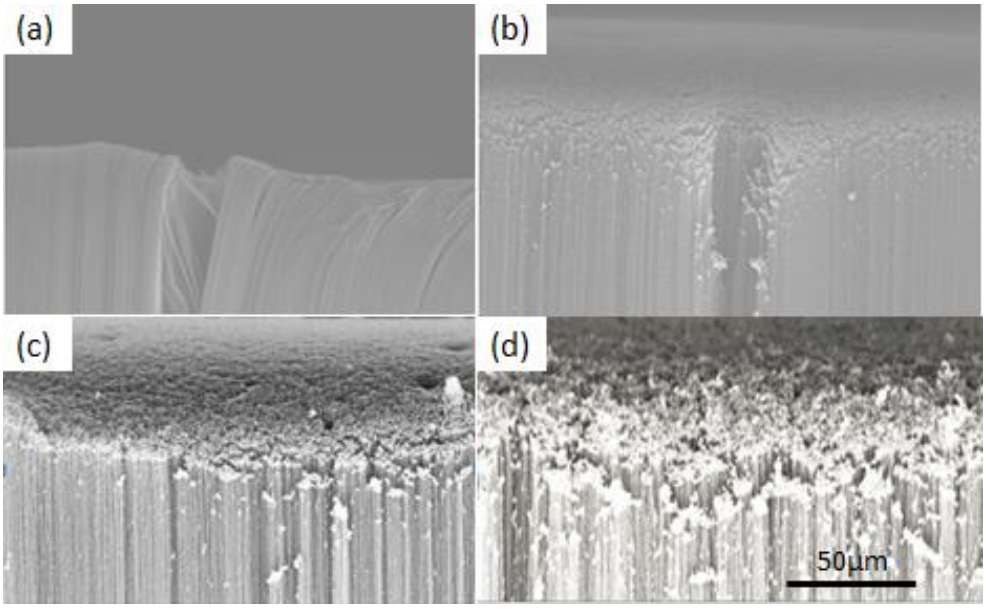

Figure 4.2 The tip part of (a) p-CNT; (b) 1min-CNT; (c) 2min-CNT; (d) 5min-CNT

The relation between the amount of liquid precursor injection and the final thickness of the VACNT array is illustrated in Figure 1.1. By applying liquid precursor in the first minute, the growth rate of CNT is nearly doubled compared to the sample with no liquid precursor at all. However, excess amount of liquid precursor greatly decrease the growth rate. It is possible that the redundant core shell units provided by the decomposition of the liquid precursor deactivate the catalyst and terminate the CNT growth.

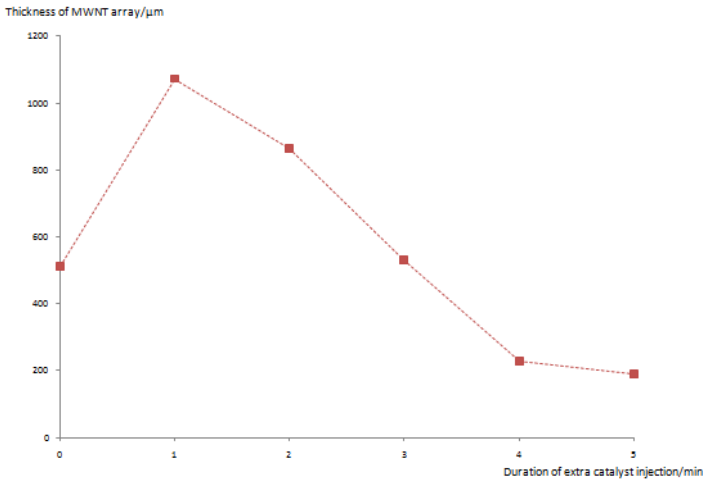

Figure 4.3 The impact of liquid precursor on the growth rate of VACNT array

If the core shell units provided by the decomposition of liquid precursors simply join with the CNTs to enhance the growth rate, then the discontinuous catalyst particles should exist in the hollows of CNTs. To clarify this hypothesis, the samples were further characterized using TEM-JEOL CX100 (**Figure 1.1**). Small amount of adhesive epoxy was carefully added to a copper grid. The grid with epoxy was then slightly pressed on the cross-section of MWNT array samples to pick up a small bundle of CNTs without disturbing the alignment. It is surprising that no Fe particles were found trapped in the cores of MWNTs. This fact indicates that the way the PAH coated Fe particles integrate in the CNT structure is different from the typical liquid precursor CVD (**Figure 1.1**). The core part of the core shell units may merge into the original catalyst particles or stay in the gas phase as extra catalyst.

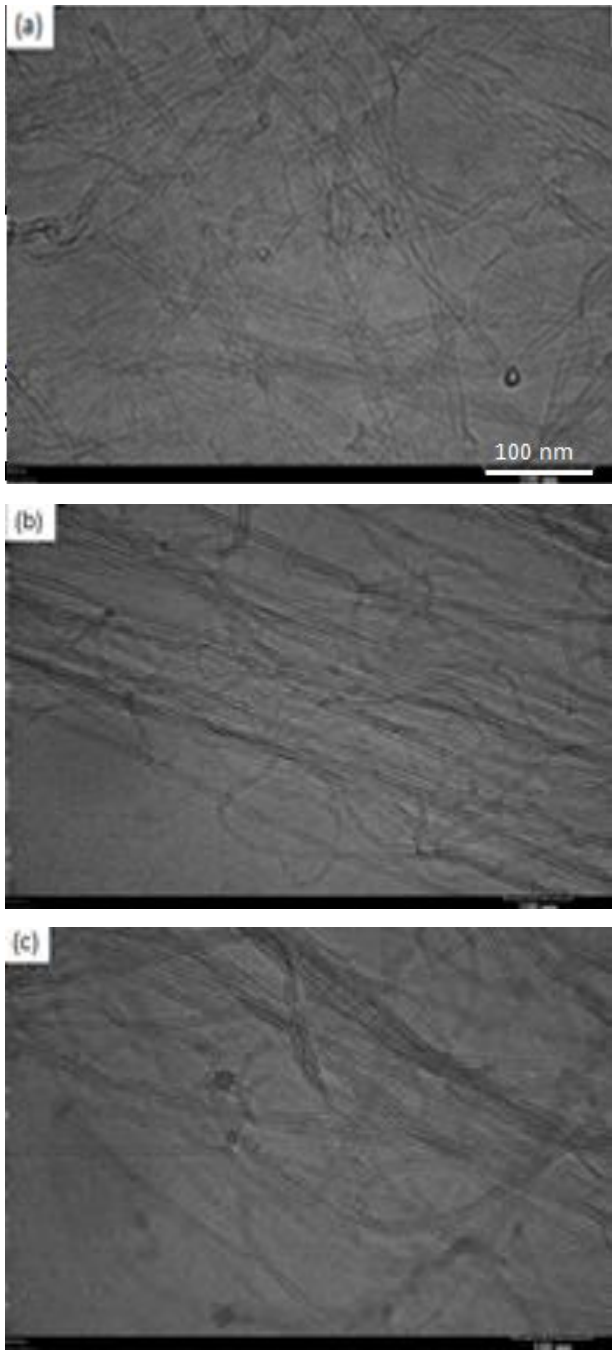

Figure 4.4 TEM images of consequent (a) root; (b) middle; (c) tip parts of VACNT array grown with extra liquid precursor.

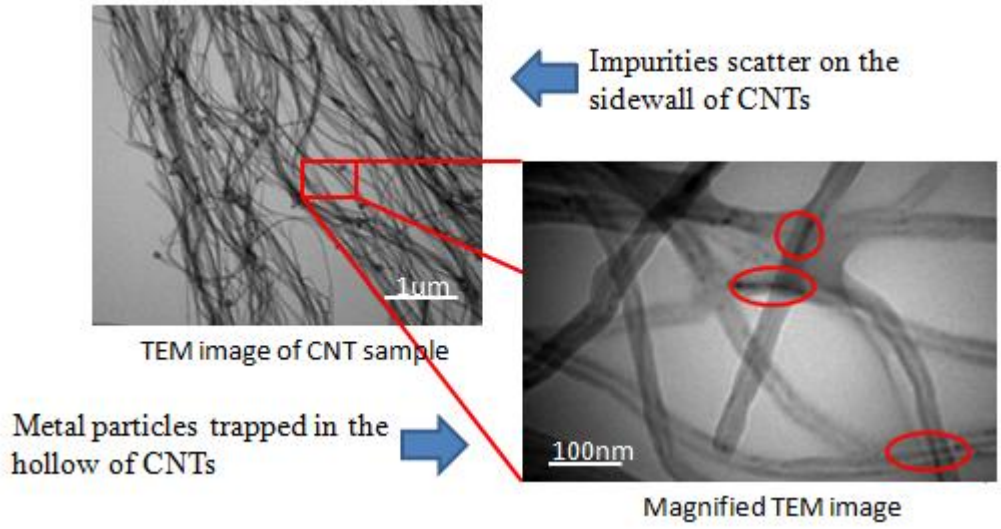

Figure 4.5 The TEM images of CNTs grown by typical liquid precursor CVD method at two levels of magnifications

The redundant core shell units may attach on the surface of the CNTs as impurities. A series of SEM images of samples grown with increasing amount of liquid precursor are present in Figure 4.2. It is clear by comparison that the more liquid precursor applied, the more impurities accumulated on the tip of CNTs. TGA data also illustrate this trend (**Figure 1.1**). As the amount of liquid precursor is increased, the quality of the CNTs first slightly gets better and then rapidly degrades. This trend further proves the role of redundant core shell units as impurities in the product. These core shell units attach on the sidewalls of CNTs and disrupt the regular hexagonal arrangement of the carbon atoms.

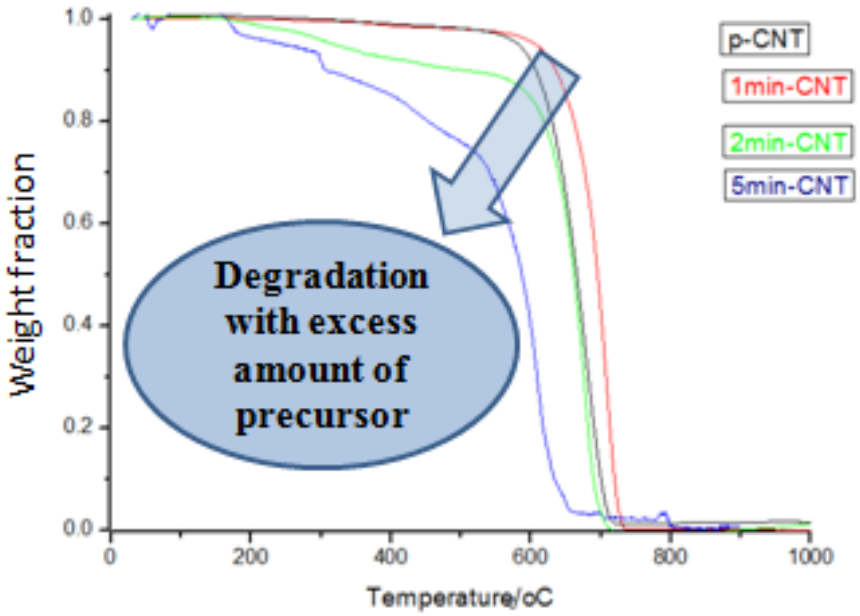

Figure 4.6 TGA data of all the samples in this section.

The D/G peak intensity ratio in Raman spectra is another convincing characterization for the evaluation of CNT quality. The D peak represents the vibration mode possessed by sp^3 bonds in the sample, while the G peak represents the ones possessed by sp^2 bonds, or graphitic structure. The higher the D/G ratio, the more defects in the graphitic structures in CNT, and the lower quality the sample. Figure 4.7 shows the D/G ratio of all the samples in this section. The trend is similar with TGA results. The D/G ratio increases with the amount of liquid precursor. It's hard to explain the slight bigger D/G ratio in 1 min-CNT sample compared to p-CNT. However, this difference falls within the error bar, which is acceptable.

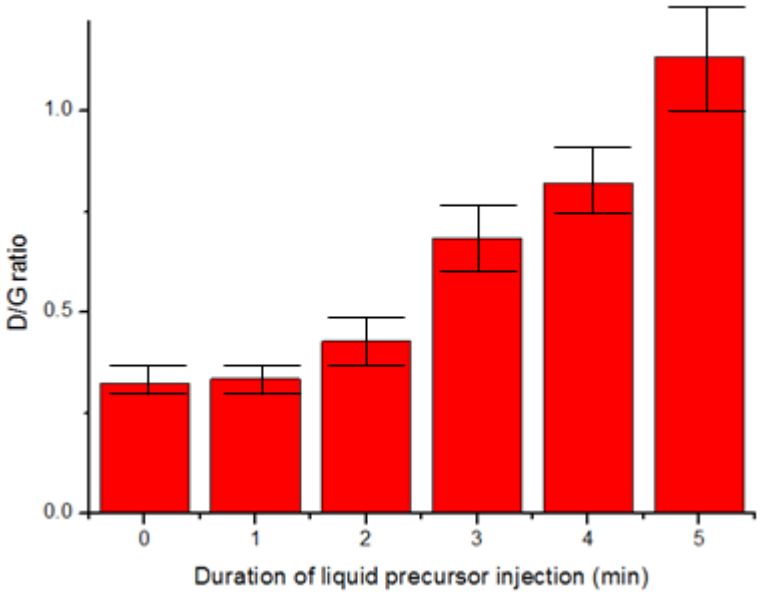

Figure 4.7 D/G ratio in the Raman spectra of all the samples in this section.

Based on the result, the mechanism of CVD growth of VACNT array supported by both gas precursor and extra liquid precursor can be concluded as the following (illustrated in **Figure 1.1**):

As the extra liquid precursor is applied, it decomposes at the high temperature. The organometallic compound such as ferrocene decomposes into catalyst particles and carbon sheets. The xylene solvent decomposes to carbon sheets as well. The carbon sheets attach on the surface of the catalyst particles and wrap them up to form core shell units. These units float in the atmosphere of the reaction tube. They are not directly built into the CNT structure. Instead, they help decompose the gas precursor to enhance the growth rate of CNT array. After the reaction, these core shell units are likely to deposit

on the tip part of CNT array as impurities. If the amount of liquid precursor exceeds the necessary amount, then more impurities are likely to attach on the sidewalls of CNT array and disrupt the regular hexagonal arrangement of the carbon atoms, introducing defects.

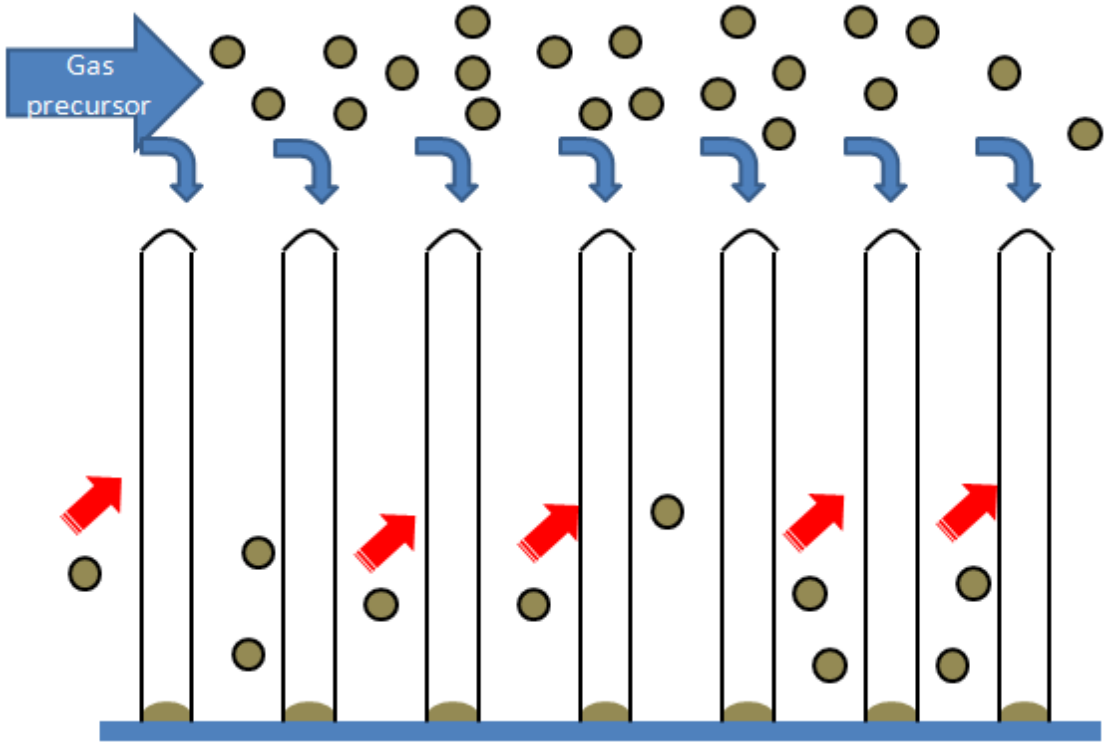

Figure 4.8 The mechanism of liquid precursor supported CVD growth of VACNT array

4.2 The effect of the total thickness of the catalyst and the cycle number

The effect of the total thickness and the cycle number of the catalyst deposition is studied. The samples are prepared by CVD method with different amount of catalyst and different cycle numbers of deposition, respectively. The nomenclature of the samples is presented in the following table:

Table 4.2 Nomenclature of the samples for the effect of catalyst thickness and cycle numbers

Number of cycles	Thickness per cycle	Sample ID
2	1	1X2
4	0.5	0.5X4
1	1	1X1
1	2	2X1
1	4	4X1

Firstly, the total amount of catalyst is varied from 0.5 to 4 nm. All other conditions are kept unchanged, including the pressure, temperature, and the gas flow. The result shows that 2 nm is the optimized catalyst thickness for CNT growth (**Figure 1.1**).

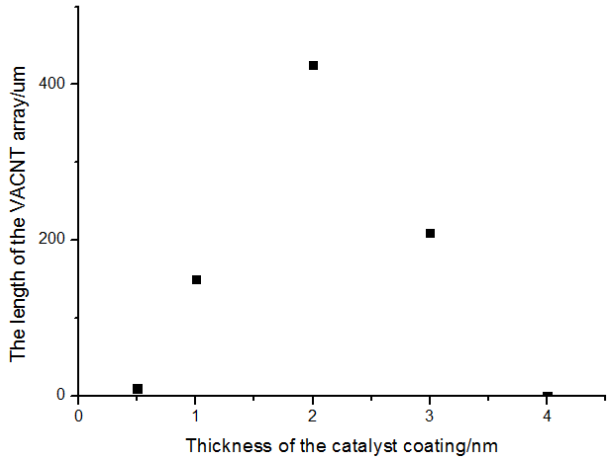

Figure 4.9 The effect of total thickness of the catalyst on the final length of the VACNT array

As the second step, the thickness of the catalyst layer is fixed as 2 nm, while the cycle number is adjusted from 1 to 4, by adjusting the thickness of deposition in each cycle. The packing density and the final thickness of the samples are monitored and recorded. The time for the CVD growth is fixed as 5 min to ensure that the termination of CNT growth is caused by intentionally shutting off the precursor. The final thicknesses of the samples are shown in **Figure 1.1**. The packing density of the samples prepared is calculated by *equation 3.1*. The result is presented in **Figure 1.1**. It is interesting to observe that with the total thickness of catalyst fixed, the growth rate decreases rapidly with the increase of cycle number, while the packing density can increase roughly by 4 fold.

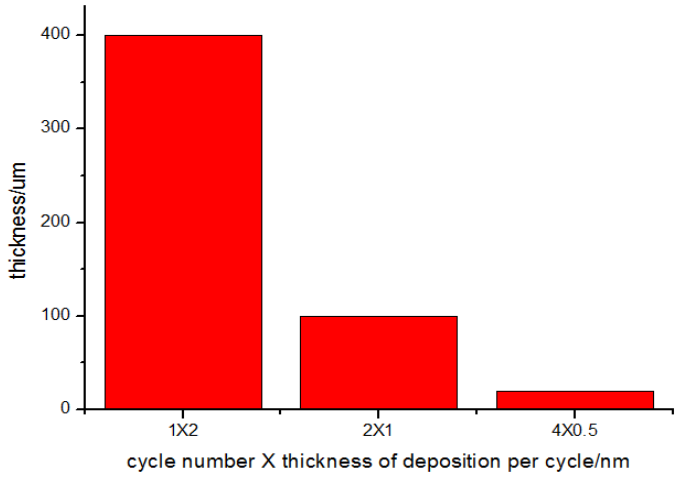

Figure 4.10 Thickness of VACNT array grown with different cycles of catalyst with total amount the same (2 nm)

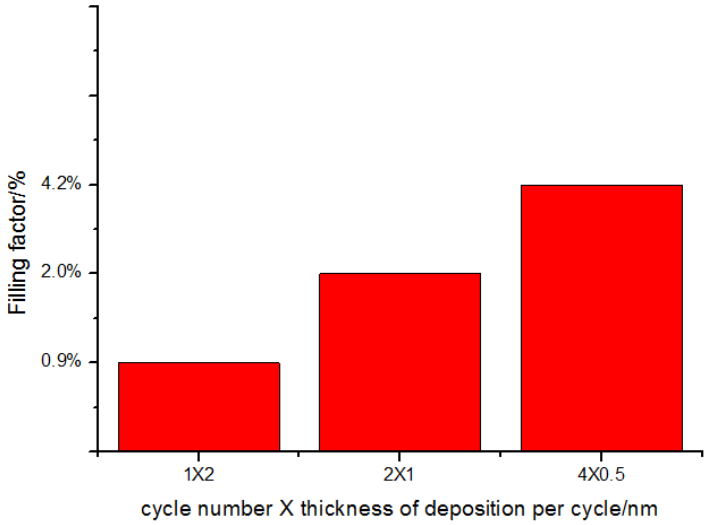

Figure 4.11 Filling factor of VACNT array grown with different cycles of catalyst with total amount the same (2 nm).

While the increase in the packing density is easy to understand, the decrease in the growth rate is more abstruse. One explanation for this could be that, as the packing density of VACNT array is increased, the diffusion length of carbon precursor through the CNT array is decreased. On the other hand, CVD growth is typically base growth, which means that the catalyst stays on the substrate rather than being lifted up to the tip of the CNTs. As a result, the growth rate is limited by the amount of carbon precursor reaching the catalyst surface at the bottom of the CNT array. However, a simple experiment rules out this possibility. A bare Si sheet is covered on the catalyst coated substrate. Then the covered substrate is located in the center of the reaction tube for CVD growth. The same condition is performed on an uncovered substrate for controlling

sample. VACNT array still results on the covered substrate, with a slightly shorter length compared to the one grown on uncovered substrate (**Figure 1.1**). This result indicates that the major mass transfer of carbon precursor for CNT growth cannot be vertical, otherwise it would have been totally blocked away by the Si sheet covered on top.

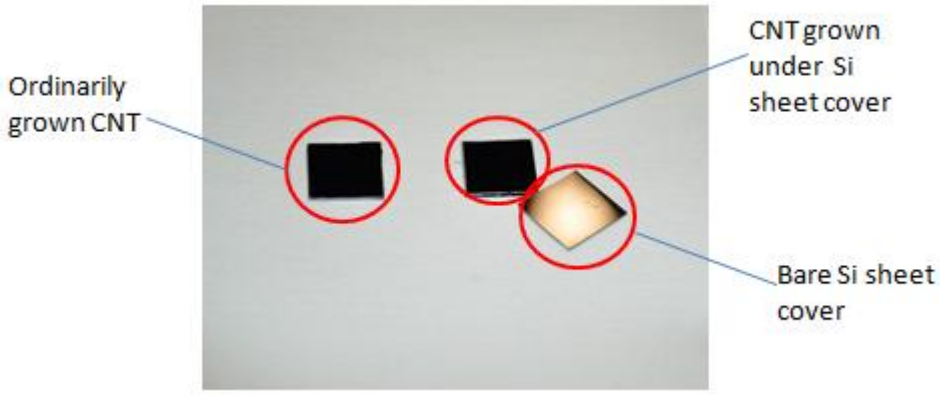

Figure 4.12 VACNT array growth with and without Si cover

In fact, the decrease of the growth rate by increasing the cycle number of catalyst deposition can be more reasonably explained by the change in the average size of the particles. By temporarily immobilizing the catalyst particles on the substrate, the Ostwald Ripening process is greatly suppressed. As a result, the average size of the catalyst particles is reduced while the total number of the catalyst particles is increased. On the other hand, the optimized temperature for CNT growth is related to the size of the catalyst particles. Therefore, the growth rate of multilayer catalysts will probably be enhanced by increasing the growth temperature. However, with the temperature increased, H_2 may become more active as reducing agent to attack the oxidation layer on the surface of the catalyst particles, so that Ostwald Ripening may be activated again. The solution to this dilemma is to apply appropriate amount of liquid precursor to enhance the growth rate at relatively low temperature, as discussed in **section 4.1**.

4.3. The impact of packing density on the thermal conductivity of VACNT array

Although the number of cycles of catalyst deposition poses significant effect on the growth rate of VACNT array, the quality of the samples does not vary much. Assuming a uniform quality of all the samples, the packing density is the only factor which differentiates the thermal conductivity of the samples. Besides increasing the packing density by applying multilayer catalyst, mechanical densification of CNT array (**Figure 1.1**) is also applied. The 1X2 sample is densified 4 times and used as the controlling sample. This sample is named as MECH.

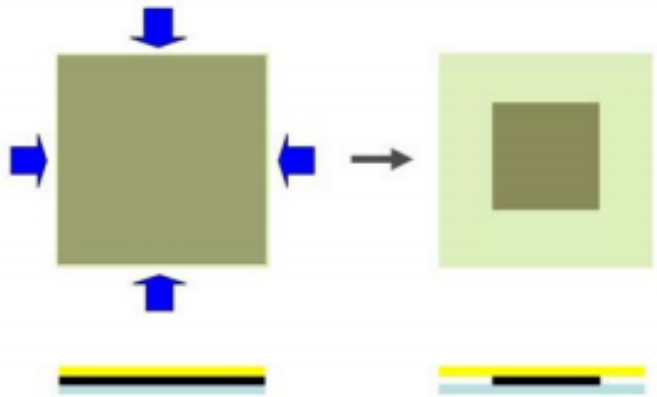

Figure 4.13 Illustration of mechanical densification of VACNT array

All the samples are adjusted to the similar thickness at around 500 microns (by changing the growth time or applying liquid precursor). The measured thermal diffusivity results of the samples are presented in the following table:

Table 4.3 Thermal diffusivity results by LFA measurement

Sample ID	Filling factor (%)	Averaged thermal diffusivity α (mm^2/s)	Calculated thermal conductivity κ (W/m K)
1X2	0.9%	48.7	45.2
2X1	2.0%	61.8	57.3
4X0.5	4.2%	81.5	75.5
MECH	4%	52.0	48.2

It is a clear trend that the thermal diffusivity of VACNT array increases with the packing density. Although MECH and 4X0.5 samples are similar in the packing density, the gap in the thermal diffusivity is caused by the misalignment from the densifying operation. According to the equation $\kappa=\alpha\rho c_p$, the thermal conductivity can be calculated. The mass density of multi-walled CNT array is around $1.3g/cm^3$, while the specific heat capacity is reported to be 713 mJ/g K. The optimized κ reaches 75.5 W/m K.

Chapter 5 CONCLUSIONS AND FUTURE WORK

The packing density of VACNT array is increased by 4 fold without quality degradation by the method of cycled deposition of catalyst for the purpose of its application in TIMs. The thermal conductivity is correspondingly increased, with the maximum value of 75.5 W/m K. On the other hand, the cycled deposition of catalyst does not only cause the increase of packing density but also slows down the growth rate, because of the change in the average size of the catalyst particles. The role of the liquid precursor in the CVD process is also systematically studied and discussed. The liquid precursor enhances the growth rate of CNTs. Excess amount of liquid precursor may cause the accumulation of impurities on the tips and even the sidewalls of the CNTs which degrades the quality of the sample.

Nevertheless, to achieve the real-life application of VACNT array in TIMs, there are still more questions to answer. Efforts should be made to further increase the filling factor to around 40% or more to confirm the real role of packing density in the thermal conductivity of VACNT array, because some theoretical work has predicted the possible thermal insulation by the coupling effect caused by too close contact between neighboring CNTs [42]. It will also be meaningful to study how to promote the quality of the VACNT arrays produced by PECVD or other methods.

I believe that this work has set a foundation to continue research and lead to a better understanding of how the thermal conductivity of the collective thermal conductivity of VACNT array is related to its geometric properties.

REFERENCES

1. Ebbesen, T.W., Large-Scale Synthesis of Carbon Nanotubes. *Nature, 1992. **358**.*

2. Iijima, S., Helical Microtubules of Graphitic Carbon. *Nature, 1991. 354*(6348).

3. Odom, T.W., Atomic Structure and Electronic Properties of Single-Walled Carbon Nanotubes. *Nature, 1998. 391*(6662).

4. Wildoer, J.W.G., Electronic Structure of Atomically Resolved Carbon Nanotubes. *Nature, 1998. 391*(6662).

5. Nyamori, V.O., S.D. Mhlanga, and N.J. Coville, The use of organometallic transition metal complexes in the synthesis of shaped carbon nanomaterials. *Journal of Organometallic Chemistry, 2008. 693*(13): p. 2205-2222.

6. Xiong, G.Y., et al., Effect of temperature, pressure, and gas ratio of methane to hydrogen on the synthesis of double-walled carbon nanotubes by chemical vapour deposition. *Nanotechnology, 2005. 16*(4): p. 532-535.

7. Bandow, S., Effect of the Growth Temperature on the Diameter Distribution and Chirality of Single-Wall Carbon Nanotubes. *Physical Review Letters, 1998. 80*(17).

8. Eres, G., Molecular Beam-Controlled Nucleation and Growth of Vertically Aligned Single-Wall Carbon Nanotube Arrays. *Journal of Physical Chemistry B, 2005. 109.*

9. Chiang, I.W., Purification and Characterization of Single-Wall Carbon Nanotubes (SWNTs) Obtained from the Gas-Phase Decomposition of CO (HiPco Process). *Journal of Physical Chemistry B, 2001. 105.*

10. Liu, J., Large-Scale Synthesis of Carbon Nanotubes by an Ethanol Thermal Reduction Process. *Journal of the American Chemical Society, 2003. 125*(27).

11. Yamada, T., Revealing the Secret of Water-Assisted Carbon Nanotube Snthesis by Microscopic Observation of the Interaction of Water on the Catalysts. *Nano letters, 2008. 8*(12).

12. Amelinckx, S., A Formation Mechanism for Catalytically Grown Helix-Shaped Graphite Nanotubes. *Science, 1994. 265*(5172).

13. Nanoparticles and Filled Capsules. *Carbon, 1995. 33*(7).

14. Gavillet, J., et al., Root-Growth Mechanism for Single-Wall Carbon Nanotubes. *Physical Review Letters, 2001. 87*(27).

15. Zhu, L., Monitoring Carbon Nanotube Growth by Formation of Nanotube Stacks and Investigation of the Diffusion'Controlled Kinetics. *Journal of Physical Chemistry B, 2006. 110.*

16. Huang, S., Growth Mechanism of Oriented Long Single Walled Carbon Nanotubes Using "Fast-Heating" Chemical Vapor Deposition Process. *Nano Letters, 2004. 4*(6).

17. Baker, R.T.K., Nucleation and Growth of Carbon Deposits from the Nickel Catalyzed Decomposition of Acetylene. *Journal of Catalysis, 1972. 26*: p. 51.

18. Yang, R.T., Evidence for Temperature-Driven Carbon Diffusion Mechanism of Coke Deposition on Catalysts. *Journal of Catalysis, 1985. 93.*

19. Li, Y., et al., Mass production of high-quality multi-walled carbon nanotube bundles on a Ni/Mo/MgO catalyst. *Carbon, 2005. 43*(2): p. 295-301.

20. Nielsen, J.R., Mechanisms of Carbon Formation on Nickel-Containing Catalysts. *Journal of Catalysis, 1977*. **48**.

21. Baird, T., Carbon Formation on Iron and Nickel Foils by Hydrocarbon Pyrolysis-Reactions at 700C. *Carbon, 1974.* **12**.

22. Latorre, N., Carbon Nanotube Growth by Catalytic Chemical Vapor Deposition: A Phenomenological Kinetic Model. *Journal of Physical Chemistry C, 2010. 114.*

23. Zhang, G., Ultra-high-yield growth of vertical single-walled carbon nanotubes: Hidden roles of hydrogen and oxygen. *Proceedings of the National Academy of Sciences, 2005. 102*(45): p. 16141-16145.

24. Hata, K., Water-Assisted Highly Efficient Synthesis of Impurity-Free Single-Walled Carbon Nanotubes. *Science, 2004. 306*(5700): p. 1362-1364.

25. Nasibulin, A., et al., An essential role of CO_2 and H_2O during single-walled CNT synthesis from carbon monoxide. *Chemical Physics Letters, 2006. 417*(1-3): p. 179-184.

26. Chiang, W.-H. and R.M. Sankaran, Synergistic Effects in Bimetallic Nanoparticles for Low Temperature Carbon Nanotube Growth. *Advanced Materials, 2008. 20*(24): p. 4857-4861.

27. Wang, S., et al., Dopants adsorbed as single atoms prevent degradation of catalysts. *Nature Materials, 2004. 3*(3): p. 143-146.

28. Cava, A.I.L., Studies of Deactivation of Metals by Carbon Deposition. *Carbon, 1982. 20*(3).

29. Iijima, S., Growth of Carbon Nanotubes. *Materials Science and Engineering B, 1993. 19.*

30. Xiang, R., Growth Deceleration of Vertically Aligned Carbon Nanotube Arrays: Catalyst Deactivation or Feedstock Diffusion Controlled? *Journal of Physical Chemistry C, 2008. 112.*

31. Han, J.-H., A Mechanochemical Model of Growth Termination in Vertical Carbon Nanotube Forests. *ACS Nano, 2008. 2*(1).

32. Bedewy, M., Collective Mechanism for the Evolution and Self-Termination of Vertically Aligned Carbon Nanotube Growth. *Journal of Physical Chemistry C, 2009. 113.*

33. Baughman, R.H., Carbon Nanotubes--the Route Toward Applications. *Science, 2002. 297*(5582): p. 787-792.

34. Berber, S., Unusually High Thermal Conductivity of Carbon Nanotubes. *Physical Review Letters, 2000. 84*(20).

35. Cao, J., et al., Thermal conductivity of zigzag single-walled carbon nanotubes: Role of the umklapp process. *Physical Review B, 2004. 69*(7).

36. Mingo, N., Carbon Nanotube Ballistic Thermal Conductance and Its Limits. *Physical Review Letters, 2005. 95.*

37. Zhang, W., et al., Chirality dependence of the thermal conductivity of carbon nanotubes. *Nanotechnology, 2004. 15*(8): p. 936-939.

38. Padgett, C.W., Influence of Chemisorption on the Thermal Conductivity of Single-Wall Carbon Nanotubes. *Nano Letters, 2004. 4*(6).

39. Hone, J., Thermal Conductivity of Single-Walled Carbon Nanotubes. *Synthetic Metals, 1999. 103.*

40. Pop, E., Thermal COnductance of an Individual Single-Wall Carbon Nanotube above Room Temperature. *Nano Letters, 2006. 6*(1).

41. Fujii, M., et al., Measuring the Thermal Conductivity of a Single Carbon Nanotube. *Physical Review Letters, 2005. 95*(6).

42. Prasher, R., et al., Turning Carbon Nanotubes from Exceptional Heat Conductors into Insulators. *Physical Review Letters, 2009. 102*(10).

43. Hone, J., Electrical and Thermal Transport Properties of Magnetically Aligned Single Wall Carbon Nanotube Films. *Applied Physics Letters, 2000. 77*(5).

44. Yang, D., et al., Thermal conductivity of multiwalled carbon nanotubes. *Physical Review B, 2002. 66*(16).

45. Wang, X., Z. Zhong, and J. Xu, Noncontact thermal characterization of multiwall carbon nanotubes. *Journal of Applied Physics, 2005. 97*(6): p. 064302.

46. Hu, X.J., et al., 3-Omega Measurements of Vertically Oriented Carbon Nanotubes on Silicon. *Journal of Heat Transfer, 2006. 128*(11): p. 1109.

47. Ngo, Q., Thermal Interface Properties of Cu-filled Vertically Aligned Carbon Nanofiber Arrays. *Nano Letters, 2004. 4*(12).

48. Xu, Y., et al., Thermal properties of carbon nanotube array used for integrated circuit cooling. *Journal of Applied Physics, 2006. 100*(7): p. 074302.

49. Tong, T., Dense vertically aligned multiwalled carbon nanotube arrays as thermal interface materials. *IEEE Transport Component Packaging Technology, 2007. 30*(1).

50. Cola, B.A., et al., Photoacoustic characterization of carbon nanotube array thermal interfaces. *Journal of Applied Physics, 2007. 101*(5): p. 054313.

51. Hu, X.J., M.A. Panzer, and K.E. Goodson, Infrared Microscopy Thermal Characterization of Opposing Carbon Nanotube Arrays. *Journal of Heat Transfer, 2007. 129*(1): p. 91.

52. Panzer, M.A., et al., Thermal Properties of Metal-Coated Vertically Aligned Single-Wall Nanotube Arrays. *Journal of Heat Transfer, 2008. 130*(5): p. 052401.

53. Lin, W., et al., Molecular phonon couplers at carbon nanotube/substrate interface to enhance interfacial thermal transport. *Carbon, 2010. 48*(1): p. 107-113.

54. Nessim, G.D., Tuning of VACNT diameter and areal density through catalyst pre-treatment. *Nano Letters, 2008. 8*(11): p. 3587-3593.

55. Hart, A.J., Rapid growth and flow mediated nucleation of millimeter scale aligned carbon nanotube structures from a thin film catalyst. *J. Phys. Chem. B, 2006. 110*: p. 8250-8257.

56. Amama, P.B., Role of Water in Super Growth of Single-Walled Carbon Nanotube Carpets. *Nano Letters, 2009. 9*(1): p. 44-49.

57. Wen, Q., W. Qian, and F. Wei, Synthesis of Single-Walled Carbon Nanotubes with Narrow Diameter Distribution by Calcination of a Mo-Modified Fe/MgO Catalyst. Chinese Journal of *Catalysis, 2008. 29*(7): p. 617-623.

58. Lamouroux, E., et al., Identification of key parameters for the selective growth of single or double wall carbon nanotubes on FeMo/Al_2O_3 CVD catalysts. *Applied Catalysis A: General, 2007. 323:* p. 162-173.

59. Cordier, A., Catalytic Chemical Vapor Deposition Synthesis of Double-Walled and Few-Walled Carbon Nanotubes by Using a MoO3-Supported Conditioning Catalyst to Control the Formation of Iron Catalytic Particles within an alpha-$Al_{1.8}Fe_{0.2}O_3$ Self-Supported Foam. *Journal of Physical Chemistry C, 2010. 114:* p. 19188-19193.

60. Parker, W.J., Flash method of determining thermal diffusivity heat capacity and thermal conductivity. *Journal of Applied Physics, 1961. 32*(9).

61. Fan, Y., et al., Single- and multi-wall carbon nanotubes produced using the floating catalyst method: Synthesis, purification and hydrogen up-take. *Carbon, 2006. 44*(11): p. 2160-2170.